

# Continuation techniques applied to the Taylor-Couette problem. Spiral flow and the stability of Taylor vortices.

J. Sánchez<sup>†</sup> and J. Antonijoan<sup>‡</sup>

<sup>†</sup> Dept. Física Aplicada. Universitat Politècnica de Catalunya.  
c/ Gran Capità s/n, Mod. B5 Campus Nord, 08034 Barcelona, Spain.  
email: sanchez@fa.upc.es

<sup>‡</sup> Dept. Matemàtica i Telemàtica. Universitat Politècnica de Catalunya.  
Av. Víctor Balaguer s/n, 08800 Vilanova i la Geltrú, Spain.  
email: fina@fa.upc.es

## Summary

We examine the spiral flow and the stability of the Taylor vortex flow in the periodic Taylor-Couette problem. We use an efficient computational scheme adapted to this problem based on continuation methods applied to an spectral discretization of the Navier-Stokes equations. We have computed the spiral flow by using an special coordinate system to exploit its symmetries and by writing the equations in the rotating reference frame where the spiral flow is steady. Taylor vortex flows are stationary so they can also be computed using continuation methods and their stability can be analyzed during the continuation process.

## 1 The Taylor-Couette problem.

The Taylor-Couette problem studies the flow of an incompressible fluid confined between two coaxial independently rotating cylinders. The geometry of the system is specified by the inner and outer radius of the cylinders  $r_i^*$  and  $r_o^*$ , with gap width  $d = r_o^* - r_i^*$ . The inner cylinder rotates with angular velocity  $\Omega_i$ , which is chosen by convention positive, and the outer cylinder rotates with angular velocity  $\Omega_o$ . The non-dimensional parameters for the problem are the radius ratio  $\eta = r_i^*/r_o^*$ , and the Reynolds numbers associated with the tangential velocity of the cylinders  $R_i = dr_i^*\Omega_i/\nu$ ,  $R_o = dr_o^*\Omega_o/\nu$ , where  $\nu$  is the kinematic viscosity. We use  $d$  as length scale and  $d^2/\nu$  as time scale. The dimensionless Navier-Stokes equations and the incompressibility condition are then

$$\partial_t \mathbf{v} + \mathbf{v} \cdot \nabla \mathbf{v} = -\nabla p + \Delta \mathbf{v}, \quad \nabla \cdot \mathbf{v} = 0. \quad (1.1)$$

We will assume infinite cylinders and periodic solutions in the axial direction, of period  $2\pi/k$ . The boundary conditions are:

$$\mathbf{v} = R_i \hat{\mathbf{e}}_\theta \quad \text{at} \quad r = r_i, \quad \text{and} \quad \mathbf{v} = R_o \hat{\mathbf{e}}_\theta \quad \text{at} \quad r = r_o. \quad (1.2)$$

## 2 The continuation algorithm

A continuation procedure has been used for the location of equilibria, to study their dependence with respect to parameters, and for detection and analysis of bifurcations ([5],[9]).

Given  $f(x, \lambda) = 0$  with

$$f : \mathcal{U} \subset \mathcal{R}^{n+1} \longrightarrow \mathcal{R}^n$$

the curves of solutions

$$x = x(s), \quad \lambda = \lambda(s)$$

have been obtained using a predictor-corrector continuation algorithm.

At each stage of the continuation process a predictor step, based on the previous known points on the curve of solutions, provides the initial guess from which a corrector step converges to a new point on it. In our code the first two predictions are made using the tangent to the curve and after, quadratic extrapolation is used based on the last three points on the curve.

Several correctors have been used. We apply Newton or chord methods as correctors to the systems

$$\left. \begin{array}{l} f(x, \lambda) = 0 \\ \lambda = \lambda_0 \end{array} \right\} \quad \text{or} \quad \left. \begin{array}{l} f(x, \lambda) = 0 \\ x_k = x_{k0} \end{array} \right\}$$

with  $x_k$  the variable that was most increased in the last continuation step ([6]) or the following method using the Moore-Penrose inverse: if  $z = (x, \lambda)$  and  $g(z) = f(x, \lambda)$  this corrector can be constructed by defining the following iterative procedure. From a given  $z^0$  lets define  $z^{k+1} = z^k + \Delta z^k$  where  $\Delta z^k$  is obtained from the conditioned extrema problem

$$\left. \begin{array}{l} \min \|\Delta z^k\|_2 \\ g(z^k) + Dg(z^k)\Delta z^k = 0 \end{array} \right\}$$

with solution

$$\Delta z^k = -Dg(z^k)^T (Dg(z^k) \cdot (Dg(z^k))^T)^{-1} g(z^k)$$

(see [7]).

Other features of the continuation process are, the automatic arc-length step size control using curvature and number of iterations, the termination criteria using windows for the variables and a user-defined function  $h(x, \lambda) = 0$ , and finally the detection of stationary bifurcations and branch switching. Stationary bifurcations can be detected from the third corrector iteration using that

$$Dg(z^k) \cdot (Dg(z^k))^T$$

is positive definite and has zero determinant only when  $rank(Dg(z^k)) < n$ , i.e., at a bifurcation point.

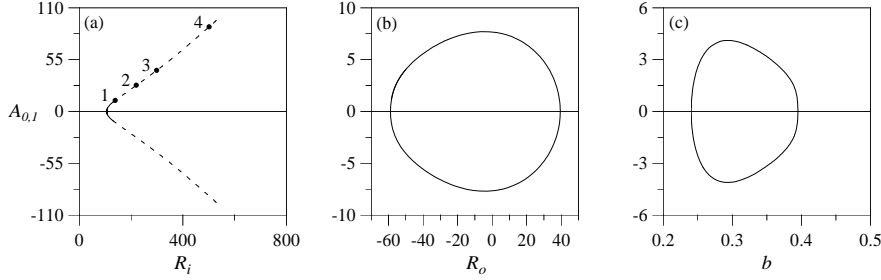


**Figure 1** Branches of spiral flow. (a) Inner Reynolds number  $R_i$  as parameter,  $b = 0.3055$  and  $R_o = -50$ , (b) Outer Reynolds number  $R_o$  as parameter,  $b = 0.3055$ , and  $R_i = 110$ , (c) Slope of spiral  $b$  as parameter,  $R_i = 110$ , and  $R_o = -50$ .

### 3 Spiral flow

The geometrical structure and symmetry properties of the spiral flow are well known ([4]). The spiral flow that appears in the counter-rotating case has a spatial structure invariant with respect to a rotation around the cylinders and a simultaneous translation in the axis direction, i.e. a helical movement which we call helical symmetry. To reduce the calculation of spirals to a 2D domain we use the system of coordinates

$$x = 2r - (r_i + r_o), \quad \theta_h = \theta, \quad \rho = z/b - \theta. \quad (3.3)$$

with  $(x, \theta_h, \rho) \in [-1, 1] \times [0, 2\pi] \times [0, 2\pi]$ .

The solutions independent of  $\theta_h$  are invariant under helical movements of the form

$$(r, \theta, z) \longrightarrow (r, \theta + \beta, z + b\beta)$$

where  $b$  is the relative magnitude of the rotation around the axis and the axial translation. We will therefore look for solutions with  $\partial_{\theta_h} = 0$  and then  $\partial_{\theta} = -\partial_{\rho}$ ,  $\partial_z = b^{-1}\partial_{\rho}$ .

The spiral flow is a travelling wave in both azimuthal and vertical directions. Therefore, to calculate them, Navier-Stokes equations have been written in a rotating frame of reference with angular velocity  $\Omega$ , in which spiral flow is steady.

To eliminate the continuity equation and the pressure from the formulation we use a representation of the velocity field using scalar potentials:

$$\mathbf{v} = f\hat{\mathbf{e}}_{\theta} + h\hat{\mathbf{e}}_z + \nabla \times (\psi\hat{\mathbf{e}}_z) + \nabla \times \nabla \times (\phi\hat{\mathbf{e}}_z)$$

where

$$f = P_{\rho}v_{\theta}, \quad h = P_{\rho}v_z \quad \text{and} \quad P_{\rho}F = \frac{1}{2\pi} \int_0^{2\pi} F(r, \rho, t) d\rho.$$

$P_\rho$  is the averaging operator in the  $\rho$  periodic coordinate. Now,  $f$  and  $h$  are only functions of  $r$ , and  $\psi$  and  $\phi$  have zero  $\rho$ -average;  $P_\rho\psi = P_\rho\phi = 0$ . The details of this formulation can be seen in Marqués [8].

The equations for  $\psi$  and  $\phi$  are obtained as the curl and double curl of Navier-Stokes equations and the ones for  $f$ ,  $h$  are  $\rho$ -averages of the former

$$\begin{aligned}(\partial_t - DD_+)f &= -P_\rho(\hat{\mathbf{e}}_\theta \cdot \mathbf{b}), \\(\partial_t - D_+D)h &= -P_\rho(\hat{\mathbf{e}}_z \cdot \mathbf{b}), \\(\partial_t - \Delta)\Delta_h\psi &= (1 - P_\rho)(\hat{\mathbf{e}}_z \cdot \nabla \times \mathbf{b}), \\(\partial_t - \Delta)\Delta\Delta_h\phi &= -(1 - P_\rho)(\hat{\mathbf{e}}_z \cdot \nabla \times \nabla \times \mathbf{b}),\end{aligned}$$

with  $\mathbf{b} = \boldsymbol{\omega} \times \mathbf{v} + 2\Omega\hat{\mathbf{e}}_z \times \mathbf{v}$ ,  $\boldsymbol{\omega} = \nabla \times \mathbf{v}$  and where the operators are  $D = \partial_r$ ,  $D_+ = D + 1/r$ ,  $\Delta_h = D_+D + r^{-2}\partial_{\rho\rho}^2$ ,  $\Delta = \Delta_h + b^{-2}\partial_{\rho\rho}^2$  and the boundary conditions

$$\left. \begin{aligned}f(r_i) &= R_i - r_i\Omega, \quad f(r_o) = R_o - r_o\Omega \\h = D\psi = \phi = \Delta_h\phi &= 0 \\-b\psi + rD\phi &= b\Delta\Delta_h\phi + rD\Delta_h\psi = 0\end{aligned} \right\} \text{ on } r = r_i, r_o.$$

The spiral flow has been computed in a wide range of parameters using continuation methods to solve the pseudo-spectral discretization ([3]) of the equations. This computational method is very well suited for studying different features of the spiral flow.

Fig. 1 shows a representation of the dependence of the solution on the parameters. We have plotted  $A_{01} = \text{sign}(\text{Re}(\psi_{0,1}))|\psi_{0,1}|$ , the absolute value of the amplitude  $\psi_{0,1}$  times the sign of its real part, versus the inner Reynolds number  $R_i$  (fig. 1a) the outer Reynolds number  $R_o$  (fig. 1b) and the slope of spiral  $b$  (fig. 1c). We have found that the spiral flow exists in a much wider parameter range than experiments suggests. In particular, it also exists in the corotating case (see fig. 1b). We have restricted the linear stability analysis of the spiral flow to perturbations with helical symmetry. Even in this case, the spirals are only stable in a small range of inner Reynolds numbers  $R_i$  (unstable branches are plotted with dashed lines in fig. 1a). To decide if these flows can be observed in the corotating case a complete stability analysis should be performed, including transitions to three-dimensional solutions.

We now consider the structure of the spirals labeled 1, 2, 3, 4 in fig. 1a corresponding to inner Reynolds number 140, 220, 300, and 500, respectively. The analysis of the flow properties shows some features very close to the ones corresponding to the Taylor vortex flow, such as formation of jet like structures (see fig. 2c) and the appearance of an inviscid core for high Reynolds number  $R_i$  (see figs. 2c and 2d).

The detailed description of the aforementioned properties and others, as particle trajectories in the spiral flow, can be seen in Antonijoan et al. [2].

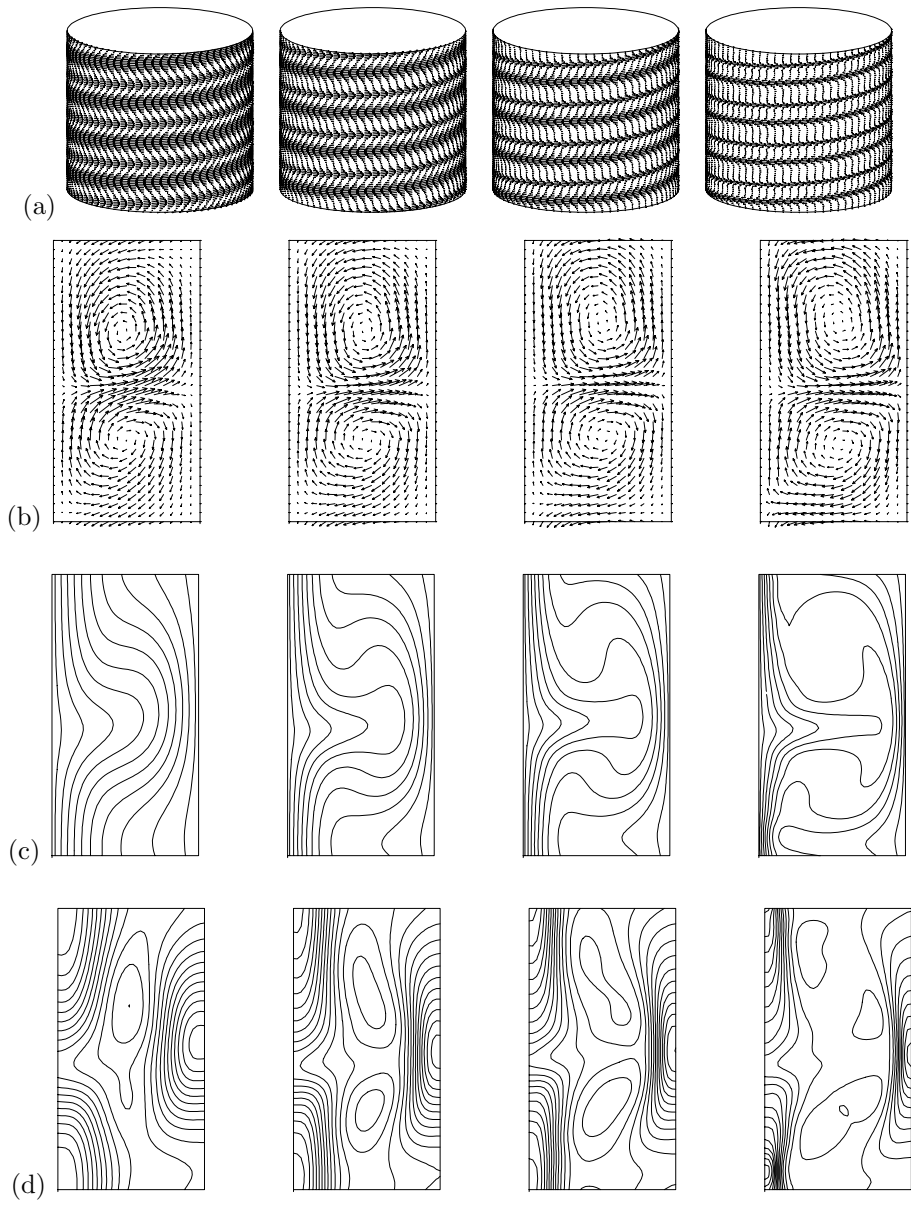


**Figure 2** (a) Perspective of the projection of the velocity field onto the mean radius surface. (b) Velocity field at a vertical plane. (c) Isolines of azimuthal velocity. (d) Isolines of vertical vorticity. The four plots in each case correspond to the spirals 1, 2, 3, and 4 along the  $R_i$  curve of Fig. 1a.

## 4 Taylor vortices and their stability

We have computed the nonlinear, steady axisymmetric solutions of the Taylor-Couette problem which correspond to Taylor vortices and examined their stability. As for the spiral flow, we will adopt a formulation based on potentials for the velocity field suited for this case. The velocity field is now written as

$$\mathbf{v} = f\hat{\mathbf{e}}_\theta + h\hat{\mathbf{e}}_z + \nabla \times (g\hat{\mathbf{e}}_\theta + \psi\hat{\mathbf{e}}_z) + \nabla \times \nabla \times (\phi\hat{\mathbf{e}}_z). \quad (4.4)$$

The main difference with the previous formulation is the appearance of the new potential  $g$  that did not appear before because of the special symmetry properties of the spiral flow ([8]).

As Taylor vortices are axisymmetric, the velocity field depends only on  $r$  and  $z$ , and the formulation can be greatly simplified;

$$\mathbf{v}_v(r, z) = f_v\hat{\mathbf{e}}_\theta + \nabla \times (g_v\hat{\mathbf{e}}_\theta)$$

with  $f_v$  and  $g_v$  verifying

$$\begin{aligned} \tilde{\Delta}f &= -g_z D_+ f + f_z D_+ g \\ \tilde{\Delta}\tilde{\Delta}g &= \frac{1}{r}\partial_z f^2 + D_+ g \tilde{\Delta}g_z - g_z D_- \tilde{\Delta}g \end{aligned}$$

The corresponding boundary conditions are

$$f(r_i) = R_i, \quad f(r_o) = R_o, \quad D_+ g = g_z = 0 \quad \text{at} \quad r = r_i, r_o$$

and the operators are

$$D = \partial_r, \quad D_\pm = D \pm \frac{1}{r}, \quad \tilde{\Delta} = DD_+ + \partial_{zz}^2.$$

Collocation methods have been used in the radial and axial coordinates.

The linear stability of the computed Taylor vortices has been studied. We consider non-axisymmetric perturbations of  $\mathbf{v}_v$  of the same axial periodicity,

$$\mathbf{v}_p(r, \theta, z, t) = \mathbf{v}_v(r, z) + \mathbf{v}(r, z)e^{\mu t}e^{im\theta} \quad (4.5)$$

being  $m \in \mathbb{Z}$  the azimuthal wave number of the perturbation. In terms of the most general scalar potentials 4.4

$$\begin{aligned} f_p(r, z, t) &= f_v(r, z) + f(r, z)e^{\mu t} \\ g_p(r, z, t) &= g_v(r, z) + g(r, z)e^{\mu t} \\ h_p(r, \theta, t) &= h(r)e^{im\theta}e^{\mu t} \\ \psi_p(r, \theta, z, t) &= \psi(r, z)e^{im\theta}e^{\mu t} \\ \phi_p(r, \theta, z, t) &= \phi(r, z)e^{im\theta}e^{\mu t}. \end{aligned}$$

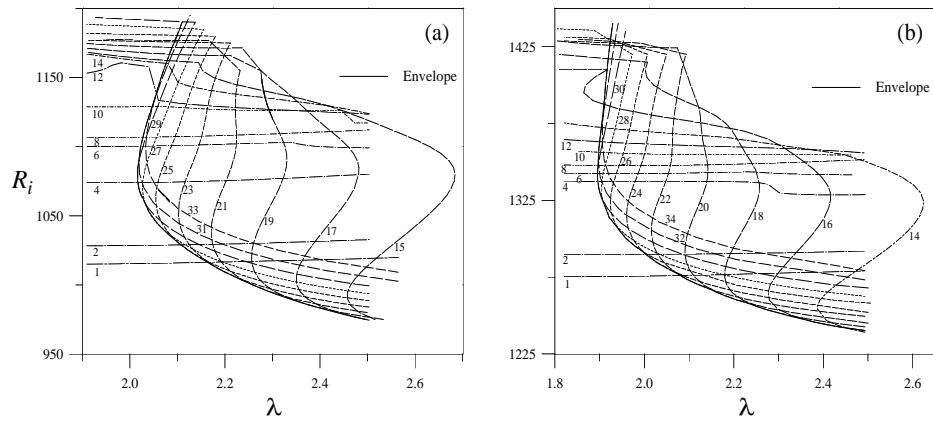


**Figure 3** The neutral stability curves from Taylor vortices corresponding to the eigenvalue problem **II**, with parameters  $\eta = 0.883$ , and Reynolds number of the outer cylinder  $R_o = 815$  in fig. 3a, and  $R_o = 1060$  in fig. 3b.

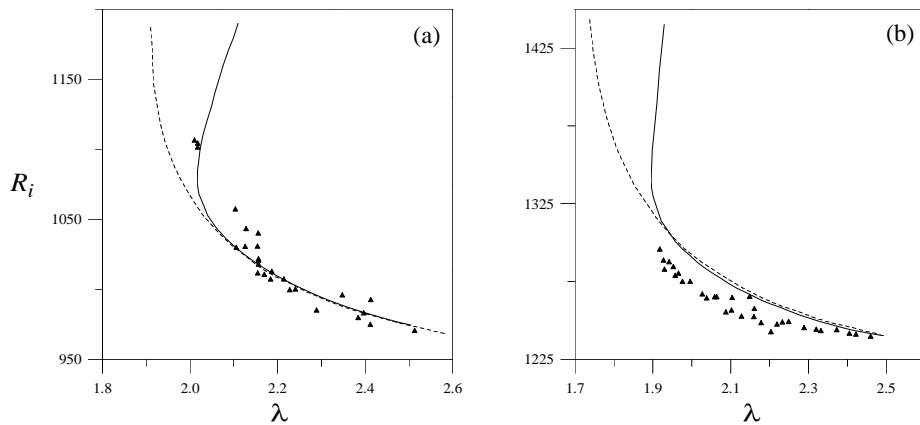


**Figure 4** The solid lines are the envelope curves shown in fig. 3a and fig. 3b. The dashed lines correspond to the calculations of Weisshaar et al. [10] and the triangles to Andereck et al. [1] experiments.

It must be noticed that  $f$  and  $g$  do not depend on  $\theta$  because they are defined as certain azimuthal averages of  $\psi$  and  $\phi$ .

It can be seen that  $f$  and  $g$  only contribute to axisymmetric instabilities that can be detected during the continuation process to calculate Taylor vortices. So we have put  $f = g = 0$ . In addition the eigenvalue problem can be splitted into two parts by separating the potentials into its even and odd parts in the vertical coordinate. If  $\psi$  and  $\phi$  are written as  $\psi = \psi^e + \psi^o$  and  $\phi = \phi^e + \phi^o$  and after substituting into the equations, a detailed study of the parity of their terms shows that the system can be separated into two kinds of eigenvalue problems: Type **I** corresponding to wavy solutions for which the perturbations are *out of phase* with the Taylor vortices:

$$\mu h(r) = \Delta_h h(r) - P_z(1 - P_\theta)\hat{\mathbf{e}}_z \cdot \mathbf{b}_{h,\psi^o,\phi^e} \quad (4.6)$$

$$\mu\Delta_h\psi^o(r, z) = \Delta\Delta_h\psi^o(r, z) + (1 - P_\theta)\hat{\mathbf{e}}_z \cdot \nabla \times \mathbf{b}_{h,\psi^o,\phi^e} \quad (4.7)$$

$$\begin{aligned} \mu\Delta\Delta_h\phi^e(r, z) &= \Delta\Delta\Delta_h\phi^e(r, z) \\ &\quad - (1 - P_\theta)(1 - P_z)\hat{\mathbf{e}}_z \cdot \nabla \times \nabla \times \mathbf{b}_{h,\psi^o,\phi^e} \end{aligned} \quad (4.8)$$

and type **II** corresponding to twisted vortices solutions for which the perturbations are *in phase* with the Taylor vortices:

$$\mu\Delta_h\psi^e(r, z) = \Delta\Delta_h\psi^e(r, z) + (1 - P_\theta)\hat{\mathbf{e}}_z \cdot \nabla \times \mathbf{b}_{\psi^e,\phi^o} \quad (4.9)$$

$$\begin{aligned} \mu\Delta\Delta_h\phi^o(r, z) &= \Delta\Delta\Delta_h\phi^o(r, z) \\ &\quad - (1 - P_\theta)(1 - P_z)\hat{\mathbf{e}}_z \cdot \nabla \times \nabla \times \mathbf{b}_{\psi^e,\phi^o} \end{aligned} \quad (4.10)$$

The set of boundary conditions for each of the eigenvalue problems are

$$h = 0 \quad (4.11)$$

$$\partial_r\psi^o = \phi^e = \Delta_h\phi^e = 0 \quad (4.12)$$

$$m\psi^o + r\partial_{rz}\phi^e = 0 \quad (4.13)$$

$$m\Delta\Delta_h\phi^e - rD\Delta_h\partial_z\psi^o = 0 \quad (4.14)$$

for **I** and

$$\partial_r\psi^e = \phi^o = \Delta_h\phi^o = 0 \quad (4.15)$$

$$m\psi^e + r\partial_{rz}\phi^o = 0 \quad (4.16)$$

$$m\Delta\Delta_h\phi^o - rD\Delta_h\partial_z\psi^e = 0 \quad (4.17)$$

for **II**, at  $r = r_i, r_o$ .

The notations  $\mathbf{b}_{h,\psi^o,\phi^e}$  and  $\mathbf{b}_{\psi^e,\phi^o}$  have been used for the term  $\mathbf{b} = \boldsymbol{\omega}_v \times \mathbf{v} + \boldsymbol{\omega} \times \mathbf{v}_v$  when the perturbation  $\mathbf{v}$  of the  $\mathbf{v}_v$  is  $\mathbf{v} = h\hat{\mathbf{e}}_z + \nabla \times (\psi^o\hat{\mathbf{e}}_z) + \nabla \times \nabla \times (\phi^e\hat{\mathbf{e}}_z)$  or  $\mathbf{v} = \nabla \times (\psi^e\hat{\mathbf{e}}_z) + \nabla \times \nabla \times (\phi^o\hat{\mathbf{e}}_z)$  respectively.

In case **II** the boundaries between vortices are not distorted and transitions to twisted vortices will be obtained. In case **I** because of the azimuthal oscillations of the boundaries, and following Weisshaar et al. [10] we will name the solutions wavy vortices or wavy twisted vortices depending on their appearance and azimuthal wave number.

The eigenvalue problems have also been solved by using a collocation method on the same mesh used to calculate Taylor vortices. The stability of each solution is obtained during the continuation process. The code that we have developed follows a curve of solutions and stops when an user-defined condition  $H(x, p) = 0$  holds. This procedure has been used with  $H$  defined as the real part of the leading eigenvalue of one of the eigenvalue problems already stated.

We have focused our attention to the transition to twisted vortices (type **II**). We have compared our results for the wide gap case with works on the narrow gap and almost corrotating cylinders case ([10]) and with experimental results ([1]).

In fig. 3a and fig. 3b we have plotted the neutral stability curves. The radius ratio is  $\eta = 0.883$  and the Reynolds number of the outer cylinder is  $R_o = 815$  and  $R_o = 1060$  respectively, as in the experiments of Andereck et al. [1]. In both figures the inner Reynolds number at which Taylor vortices become unstable is plotted against the axial wave length  $\lambda$  of the perturbed vortex for different azimuthal modes  $m$ . We show only some of the curves in the range  $1 \leq m \leq 30$  and the envelope of some of them. In fig. 3a the first unstable mode is  $m = 1$  for axial wave lengths below approximately 2.15 and above this value, the critical azimuthal wavenumber  $m$  decreases with the axial wave length starting with  $m = 25$ .

In fig. 4a and fig. 4b the triangles correspond to Andereck et al. [1] experiments, the dashed lines to the calculations of Weisshaar et al. [10] and the solid lines are the envelopes plotted in the previous figures. The correspondence between the two numerical calculations is very good for a wide range of wave lengths  $\lambda$  but our calculations match better the minimum value of  $\lambda$  at which twisted vortices are observed in experiments.

There is a vertical shift between the calculated transition curves and the experiments from [1]. It could be thought that these shifts were due to the narrow gap approximation used in [10]. We have shown that this is not the case. The only possible explanation is that they must be due to the cylinders finite length effect.

In order to obtain a picture of the flow pattern near the bifurcation point, we have added some small multiple of the velocity perturbation field to the basic axisymmetric flow. Fig. 5a shows a perspective view of the axisymmetric flow, and fig. 5b of the perturbed velocity field onto a cylindrical surface for  $r = 0.9(r_o - r_i) + r_i$ . Fig. 5b shows a pattern very similar to the experimental ones found by Andereck et al. [1] in the twisted vortices regime.

## Acknowledgments

This work was partially supported by DGICYT grant PB97-0685, and by a CESCA computing time grant.

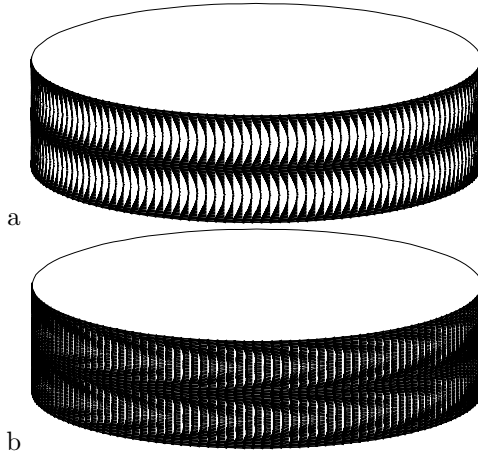


**Figure 5** Perspective views of the projection of (a) the velocity field of Taylor vortices and of (b) the perturbed velocity field corresponding to twisted vortices, onto cylindrical surfaces for  $r = 0.9(r_o - r_i) + r_i$ .

## Bibliography

- [1] C.D. Andereck, R. Dickman, and H.L. Swinney, *New flows in a circular Couette system with co-rotating cylinders*, Phys. Fluids **26**(6), 1395-1401 (1983).
- [2] J. Antoni Joan, F. Marqués, J. Sánchez. *Nonlinear spirals in the Taylor–Couette problem*, Phys. Fluids **10**(4) (1998).
- [3] C. Canuto, M.Y. Hussaini, A. Quarteroni and T.A. Zang, *Spectral Methods in Fluid Dynamics*, Springer-Verlag (1987).
- [4] P. Chossat and G. Iooss, *The Couette-Taylor problem*, Springer-Verlag, (1994).
- [5] H.B. Keller, *Numerical solution of bifurcation and nonlinear eigenvalue problems*, in *Applications of Bifurcation Theory* (ed. P.H. Rabinowitz), Academic Press (1977).
- [6] M. Kubišek, I. Marek, *Computational methods in bifurcation theory and dissipative structures*, Springer-Verlag (1983).
- [7] Y.A. Kuznetsov, *Elements of applied bifurcation theory*, Springer-Verlag (1995).
- [8] F. Marqués, *On boundary condition for velocity potentials in confined flows: Application to Couette flow*, Phys. Fluids A **2**, 729-737 (1990).
- [9] R. Seydel, *Practical bifurcation and stability analysis*, Springer-Verlag (1994).
- [10] E. Weisshaar, F.H. Busse and M. Nagata, *Twist vortices and their instabilities in the Taylor-Couette system*, J. Fluid Mech. **226**, 549-564 (1991).